


Article

DFT Calculations of ^1H NMR Chemical Shifts of Geometric Isomers of Conjugated Linolenic Acids, Hexadecatrienyl Pheromones, and Model Triene-Containing Compounds: Structures in Solution and Revision of NMR Assignments

Themistoklis Venianakis, Christina Oikonomaki, Michael G. Siskos *, Alexandra Primikyri and Ioannis P. Gerothanassis * 

Section of Organic Chemistry and Biochemistry, Department of Chemistry, University of Ioannina, GR-45110 Ioannina, Greece; t.venianakis@uoi.gr (T.V.); pch01328@uoi.gr (C.O.); a.primikyri@uoi.gr (A.P.)
* Correspondence: msiskos@uoi.gr (M.G.S.); igeroth@uoi.gr (I.P.G.)



Citation: Venianakis, T.; Oikonomaki, C.; Siskos, M.G.; Primikyri, A.; Gerothanassis, I.P. DFT Calculations of ^1H NMR Chemical Shifts of Geometric Isomers of Conjugated Linolenic Acids, Hexadecatrienyl Pheromones, and Model Triene-Containing Compounds: Structures in Solution and Revision of NMR Assignments. *Molecules* **2021**, *26*, 3477. <https://doi.org/10.3390/molecules26113477>

Academic Editor: Mauricio Alcolea Palafox

Received: 18 May 2021
Accepted: 4 June 2021
Published: 7 June 2021

Publisher's Note: MDPI stays neutral with regard to jurisdictional claims in published maps and institutional affiliations.



Copyright: © 2021 by the authors. Licensee MDPI, Basel, Switzerland. This article is an open access article distributed under the terms and conditions of the Creative Commons Attribution (CC BY) license (<https://creativecommons.org/licenses/by/4.0/>).

Abstract: A DFT study of the ^1H NMR chemical shifts, $\delta(^1\text{H})$, of geometric isomers of 18:3 conjugated linolenic acids (CLnAs), hexadecatrienyl pheromones, and model triene-containing compounds is presented, using standard functionals (B3LYP and PBE0) as well as corrections for dispersion interactions (B3LYP-D3, APFD, M06–2X and ωB97XD). The results are compared with literature experimental $\delta(^1\text{H})$ data in solution. The closely spaced “inside” olefinic protons are significantly more deshielded due to short-range through-space $\text{H} \cdots \text{H}$ steric interactions and appear close to or even beyond δ -values of aromatic systems. Several regularities of the computational $\delta(^1\text{H})$ of the olefinic protons of the conjugated double bonds are reproduced very accurately for the lowest-energy DFT-optimized single conformer for all functionals used and are in very good agreement with experimental $\delta(^1\text{H})$ in solution. Examples are provided of literature studies in which experimental resonance assignments deviate significantly from DFT predictions and, thus, should be revised. We conclude that DFT calculations of ^1H chemical shifts of trienyl compounds are powerful tools (i) for the accurate prediction of $\delta(^1\text{H})$ even with less demanding functionals and basis sets; (ii) for the unequivocal identification of geometric isomerism of conjugated trienyl systems that occur in nature; (iii) for tackling complex problems of experimental resonance assignments due to extensive signal overlap; and (iv) for structure elucidation in solution.

Keywords: CLnAs; hexadecatrienyl pheromones; chemical shifts; DFT; GIAO; NMR

1. Introduction

Conjugated linolenic acids (CLnAs) are a group of positional and geometric isomers of octadecatrienoic acids (C18:3) that contain three conjugated double bonds primarily in positions $\Delta 9,11,13$ and $\Delta 8,10,12$ [1,2]. α -Eleostearic acid (α -ESA) has three conjugated double bonds (C18:3 $\Delta 9$ *cis*, 11 *trans*, 13 *trans*) (Figure 1) and it is produced and stored in the seed oil of plants such as *A. fordii*, *M. charantia*, *Parinarium* spp., and *P. mahaleb*. α -ESA was reported to have anticancer properties on several tumor cell lines, such as A549 (lung), MCF-7 (breast), DLD1 (colorectal), MKN-7 (stomach), and HepG2 (hepatoma). Lipid peroxidation has been suggested as the underlying mechanism [3]. β -Eleostearic acid (β -ESA) (C18:3 $\Delta 9$ *trans*, 11 *trans*, 13 *trans*) (Figure 1) is present in pomegranate, bitter gourd, and *catalpa* [4]. β -ESA was reported to have a stronger antiproliferative effect than the geometric isomer α -ESA. A decrease in Bcl-2 and an increase in Bax mRNA expression along with DNA fragmentation were observed, which indicates different signaling pathways than their *cis* isomers [5]. Punicic acid (PA) (C18:3 $\Delta 9$ *cis*, 11 *trans*, 13 *cis*; Figure 1) is a fatty acid derived from the fruit of *P. granatum* (aspomegranate) and from *T. kirilowii*. PA has been reported to have several health benefits such as anticancer activity and the prevention of

obesity and insulin resistance in mice [6–8]. The cytotoxic properties on human monocytic leukemia cells have been attributed to lipid peroxidation [9].

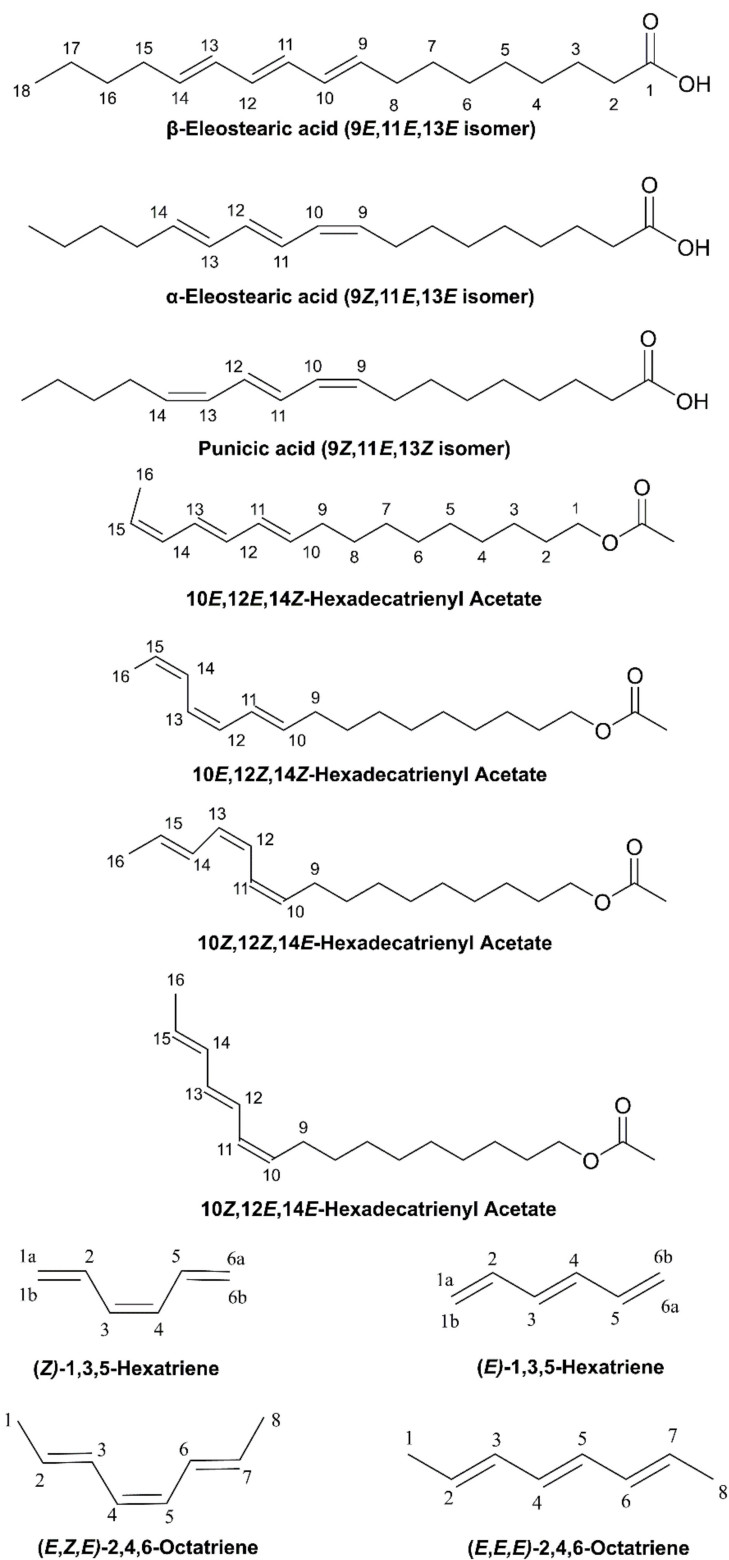


Figure 1. Chemical structures of three geometric isomers of the 18:3 ω -5 conjugated linolenic acid, four geometric isomers of the 16:3 ω -2 conjugated hexadecatrienyl acetate, and triene-containing model compounds investigated in the present work.

Molecules with three conjugated double bonds have also been identified in hexadecatrienyl systems (Figure 1) from several lepidopterous species [10]. These sex hormones from females attract male moths and, thus, have significant roles in forest ecology, human health, and communication biology [11]. Pheromone-baited traps, therefore, have been widely used for the detection, population monitoring, and control of pest species and for assessing the efficacy of eradication efforts [12]. Isolation and identification of sex pheromones, however, is a difficult task due to the very small amount of pheromone produced by the insects and the small number of individuals available for the analysis of the pheromone gland content [12]. Initially, the isomeric configuration of the natural trienals was unknown and their identity was investigated by synthesis and the use of NMR spectroscopy [13–15]. Several geometric isomers, however, are not amenable to complete resonance assignment due to extensive signal overlap.

Hexadecatrienyl pheromones and their synthetic analogues [11,13–15], conjugated linolenic acids (CLnAs) [16–20], and model triene-containing compounds [21–24] have been extensively investigated using ^1H and ^{13}C NMR. 2D-NOESY experiments, ^{13}C - ^1H COSY correlations, and analysis of spin–spin coupling constants with the use of homonuclear decoupling techniques were used to identify the geometric configurations of the trienyl conjugated double bonds. However, in several cases, severe overlap in the NMR spectra leads to equivocal signal assignments even when using 2D spectra and, consequently, to ambiguities in the spectral interpretations.

Several studies have been published that combine experimental NMR chemical shifts with computations for tackling the complex problems of resonance assignment, resonance reassignment, and structural revision [25–37] and for investigating high-resolution structures in solution [38–47]. DFT calculations of NMR chemical shifts in conjugated systems, however, are limited to ^1H and ^{13}C NMR chemical shifts of retinal isomers [48], and geometric isomers of diene-containing compounds [47]. Since no X-ray structures of conjugated linolenic acids (CLnAs) and hexadecatrienyl pheromones have so far been published, it would be of interest to use quantum chemical calculations of $\delta(^1\text{H})$ for structure elucidation in solution. In this paper, we discuss (i) the effect of various functionals and basis sets on the accuracy of the DFT calculation of ^1H NMR chemical shifts using the GIAO [49] technique on several geometric conjugated linolenic acids, hexadecatrienyl pheromones, and model triene-containing compounds (Figure 1); (ii) the use of $\delta(^1\text{H})$ for the unequivocal assignment of geometric isomerism and revision of literature experimental assignments; and (iii) the use of $\delta(^1\text{H})$ as a tool for structure elucidation in solution.

2. Results and Discussion

2.1. DFT-Calculated vs. Experimental ^1H NMR Chemical Shifts of Model Compounds in Solution: Effects of Various Functionals and Basis Sets

The experimental ^1H NMR chemical shifts of the trienyl model compounds (*Z*)-1,3,5-hexatriene, (*E*)-1,3,5-hexatriene, (*E,Z,E*)-2,4,6-octatriene and (*E,E,E*)-2,4,6-octatriene (Figure 1 and Table 1) exhibit resonances of the olefinic protons of the conjugated double bonds in the range of 5.0 to 6.8 ppm. The $=\text{CH}_2$ protons are shielded with respect to the rest of the olefinic protons and appear in a narrow range of 5.05 to 5.23 ppm. Alkyl substitution of the H_{1a} proton, as in the case of (*E,Z,E*)-2,4,6-octatriene, results in a deshielding of ~ 0.5 ppm, which is in excellent agreement with ^1H additive contribution to ethylene of $\Delta\delta_{\text{gem}} = 0.45$ ppm [50]. Interestingly, the closely spaced “inside” olefinic 2,5 protons of (*Z*)-1,3,5-hexatriene and 3,6 protons of (*E,Z,E*)-2,4,6-octatriene (Figure 1) are the most deshielded and appear close to or even beyond δ -values of aromatic systems. This deshielding effect can be attributed to rigid geometries and significant $\text{H}\cdots\text{H}$ van der Waals repulsive effects of specific protons [22]. It has been demonstrated that hydrogen atoms, which are subject to significant steric compression, exhibit a deshielding that is dependent on the geometrical relationship between the H–C bond and the interacting proximate hydrogen [51]. This occurs because the symmetry of the electron cloud about the proton is disturbed, thus resulting in reduced electronic charge and diamagnetic shielding [52,53].

Trienyl model compounds, therefore, are ideally suited for the study of steric effects on $\delta(^1\text{H})$ using various functionals and basis sets. Energy minimization of the structures was performed with standard functionals (B3LYP and PBE0) as well as with corrections for dispersion interactions (B3LYP-D3, APFD, M06-2X, and ω B97XD). Inclusion of nonlocal van der Waals density functionals has been shown to improve the accuracy of standard DFT functionals [54,55]. The 6-31+G(d) and 6-311++G(d,p) basis sets were used to compare the results of a low computational cost basis set with a medium-size one. Computations of $\delta_{\text{calc}}(^1\text{H})$ were performed (a) using a single methodology at the GIAO/B3LYP/6-311+G(2d,p)/CPCM level (Figure S1 and Figure S2 and Table S1), as recommended in [28], and (b) using the same level of theory as geometry optimization (Figure 2, Figure S3, and Table S2).

Table 1. Literature experimental ^1H NMR chemical shifts, δ_{exp} , and the sample and spectral specifications of the compounds of Figure 1.

| Group | A | B | C | D | E | F | G | H | I | J | K | L | M | | |
|-------|-----------------------------|-----------------------------|-----------------------------|-----------------------------|-------|-----------------------------|-----------------------------|-------|-----------------------------|-----------------------------|-----------------------------|-------|-----------------------------|-----------------------------|-----------------------------|
| | δ_{exp} (ppm) | δ_{exp} (ppm) | δ_{exp} (ppm) | δ_{exp} (ppm) | Group | δ_{exp} (ppm) | δ_{exp} (ppm) | Group | δ_{exp} (ppm) | δ_{exp} (ppm) | δ_{exp} (ppm) | Group | δ_{exp} (ppm) | δ_{exp} (ppm) | δ_{exp} (ppm) |
| H1a | 5.15 | 5.1 | 5.09 | 5.05 | H1 | 1.8 | 1.84 | H9 | 2.09 | 2.12 | 2.18 | H11 | 6.10 | 6.19 | 6.48 |
| H1b | 5.24 | 5.23 | 5.17 | 5.18 | H2 | 5.7 | 5.69 | H10 | 5.70 | 5.74 | 5.48 | H12 | 6.10 | 6.40 | 6.48 |
| H2 | 6.8 | 6.36 | 6.74 | 6.3 | H3 | 5.83 | 6.12 | H11 | 6.10 | 6.50 | 6.43 | H10 | 6.04 | 6.01 | 6.08 |
| H3 | 6.0 | 6.22 | 5.93 | 6.16 | H4 | 6.5 | 6.10 | H12 | 6.18 | 5.98 | 6.13 | H13 | 6.04 | 6.12 | 6.08 |
| H4 | 6.0 | 6.22 | 5.93 | 6.16 | H5 | 6.5 | 6.10 | H13 | 6.41 | 6.16 | 5.96 | H9 | 5.66 | 5.4 | 5.46 |
| H5 | 6.8 | 6.36 | 6.74 | 6.3 | H6 | 5.83 | 6.12 | H14 | 6.02 | 6.46 | 6.52 | H14 | 5.66 | 5.74 | 5.46 |
| H6a | 5.15 | 5.1 | 5.09 | 5.05 | H7 | 5.7 | 5.69 | H15 | 5.47 | 5.56 | 5.75 | H2 | 2.37 | 2.40 | 2.37 |
| H6b | 5.24 | 5.23 | 5.17 | 5.18 | H8 | 1.8 | 1.84 | H16 | 1.76 | 1.77 | 1.80 | H8 | 2.10 | 2.20 | 2.22 |
| | | | | | | | | | | | | H15 | 2.10 | 2.20 | 2.22 |
| | | | | | | | | | | | | H3 | 1.65 | 1.64 | 1.65 |
| | | | | | | | | | | | | H4 | 1.39 | 1.41 | 1.39 |
| | | | | | | | | | | | | H5 | 1.39 | 1.41 | 1.39 |
| | | | | | | | | | | | | H6 | 1.39 | 1.41 | 1.39 |
| | | | | | | | | | | | | H7 | 1.39 | 1.41 | 1.39 |
| | | | | | | | | | | | | H16 | 1.33 | 1.33 | 1.32 |
| | | | | | | | | | | | | H17 | 1.33 | 1.33 | 1.32 |
| | | | | | | | | | | | | H18 | 0.91 | 0.97 | 0.94 |

^A (Z)-1,3,5-hexatriene (CDCl₃), ^1H and 2D ^1H - ^1H COSY NMR (270 MHz) [15]; ^B (E)-1,3,5-hexatriene (CDCl₃), ^1H and 2D ^1H - ^1H COSY NMR (270 MHz) [15]; ^C (Z)-1,3,5-hexatriene (CCl₄), ^1H NMR (100 MHz) [21,22]; ^D (E)-1,3,5-hexatriene (CCl₄), ^1H NMR (100 MHz) [21,22]; ^E (E,Z,E)-2,4,6-octatriene (CDCl₃), ^1H NMR (300 MHz) [23]; ^F (E,E,E)-2,4,6-octatriene (CCl₄), ^1H NMR (100 MHz) [21]; ^G 10E,12E,14Z-hexadecatrienyl acetate (CDCl₃), ^1H , ^{13}C , and 2D ^1H - ^1H COSY NMR (270 MHz) [13]; ^H 10E,12Z,14Z-hexadecatrienyl acetate (CDCl₃), ^1H , ^{13}C , and 2D ^1H - ^1H COSY NMR (270 MHz) [13]; ^I 10Z,12Z,14E-hexadecatrienyl acetate (CDCl₃), ^1H , ^{13}C , and 2D ^1H - ^1H COSY NMR (270 MHz) [13]; ^J 10Z,12E,14E-hexadecatrienyl acetate (CDCl₃), ^1H , ^{13}C , and 2D ^1H - ^1H COSY NMR (270 MHz) [13]; ^K β -eleostearic acid (CDCl₃), ^1H , ^{13}C , and 2D ^1H - ^1H COSY NMR (400 MHz) [18]; ^L α -eleostearic acid (CDCl₃), ^1H , ^{13}C , and 2D ^1H - ^1H COSY NMR (400 MHz) [18]; ^M punicic acid (CDCl₃), ^1H , ^{13}C , and 2D ^1H - ^1H COSY NMR (400 MHz) [18].

For all the functionals and basis sets used, the literature experimental chemical shifts of the closely spaced “inside” olefinic protons with $\delta(\text{H}(3,6)) = 5.83$ ppm and $\delta(\text{H}(4,5)) = 6.50$ ppm of (E,Z,E)-2,4,6-octatriene [23] strongly deviate from linearity (Figure S2A and Figure S3A). Revision of the literature experimental chemical shift data so that the inner H(3,6) protons to be deshielded to a larger degree than H(4,5) (Figure S2B and Figure S3B) results in very significant improvements of the regression coefficients and standard deviations for all the functionals and basis sets used (Table S3 and Table S4). The use of several DFT functionals with distinct contributions (long-range corrections or dispersion interactions) would provide distinct results for the geometry. The use, however, of a single methodology at the GIAO/B3LYP/6-311+G(2d,p) level for chemical shift computations results in identical correlations coefficients and mean square errors for all the functionals and basis sets used (Table S3). The use of the same level of theory in $\delta_{\text{calc}}(^1\text{H})$ as geometry optimization results in similar but not identical statistical data (Table S4). The quality of the linear regression procedure is a criterion whether the computational method is able to reproduce the experimental chemical shifts free from random error [28]. Furthermore, the extent to which the slope of the correlation line deviates from unity and the intercept from zero is a measure of the overall systematic error. Among the functionals with corrections for dispersion interactions, the ω B97XD with the 6-31+G(d) basis set performs better

(intercept: 0.003, slope: 1.046; Table S4). The M06-2X functional is less suitable for shielding calculations of the selected molecules in agreement with literature data on several small molecules [56].

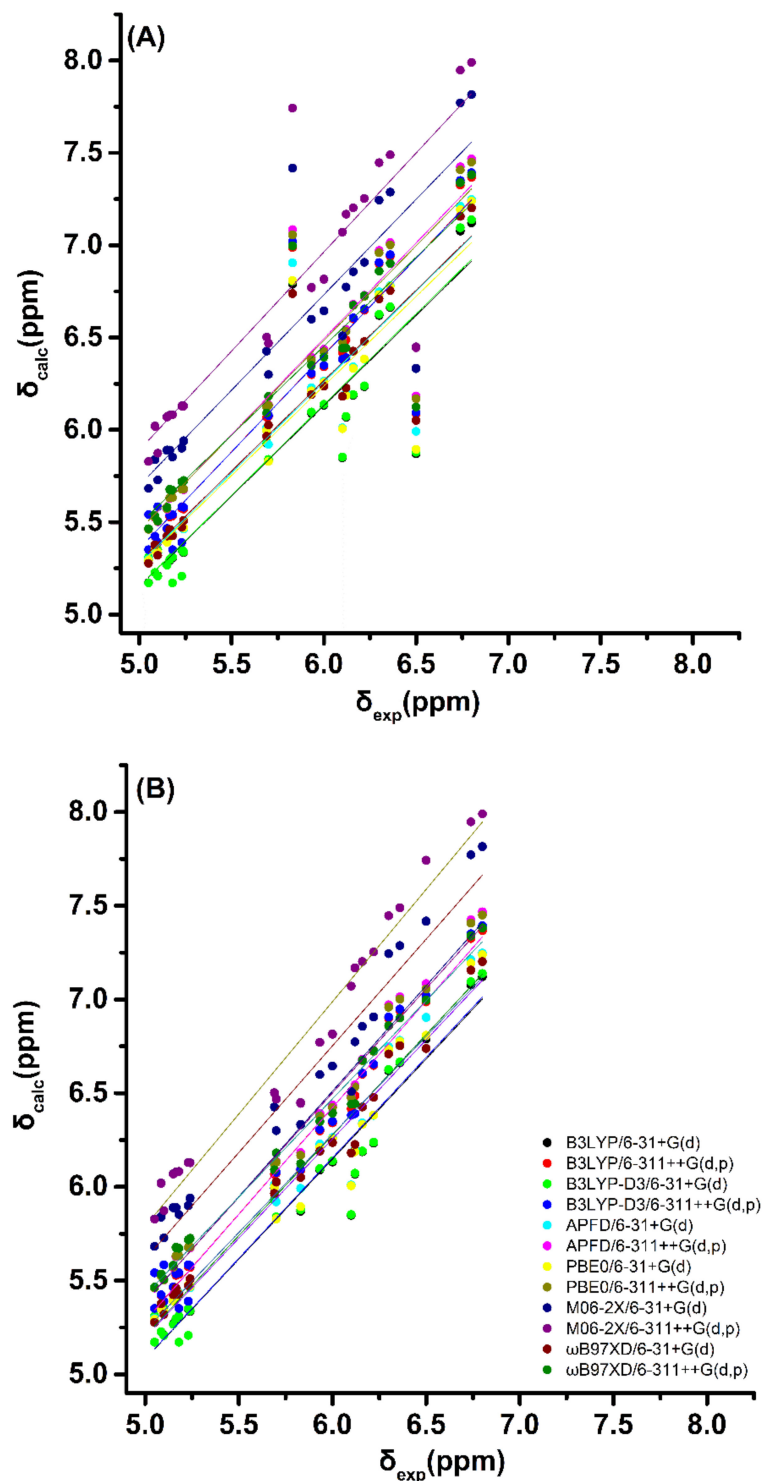


Figure 2. (A) Calculated, δ_{calc} , ^1H NMR chemical shifts with CPCM of the olefinic protons vs. experimental, δ_{exp} , chemical shifts using the same level of theory as geometry optimization for the model trienyl compounds (*Z*)-1,3,5-hexatriene, (*E*)-1,3,5-hexatriene, (*E,Z,E*)-2,4,6-octatriene, and (*E,E,E*)-2,4,6-octatriene. (B) The same as in (A), but the literature experimental values of $\delta(\text{H}(3,6)) = 5.83$ ppm and $\delta(\text{H}(4,5)) = 6.50$ ppm of (*E,Z,E*)-2,4,6-octatriene [23] have been reversed.

From the above, it can be concluded that the accuracy of the DFT calculations can provide a practical guide for future experimental assignments and help in the reassignment of literature experimental ^1H NMR chemical shifts of triene-containing compounds based on a typical workflow that includes the following steps:

- (i) the ^1H NMR spectra are recorded in, e.g., a CDCl_3 solution at 298 K, and a preliminary assignment is performed using a variety of 1D and 2D NMR experiments;
- (ii) the ^1H NMR chemical shifts are computed with the CPCM model at the same level of theory as geometry optimization or at the GIAO/B3LYP/6-311+G(2d,p) level, even with less demanding functionals and basis sets;
- (iii) a very good linear correlation between experimental NMR chemical shifts, δ_{exp} , and calculated shifts, δ_{calc} , provides a strong indication that the assignment procedure is correct.

2.2. Out-of-Plane Deformation of the Trienyl System and Steric Effects in Model Compounds

Variation of the torsion angle $\varphi(\text{C}_1, \text{C}_2, \text{C}_3, \text{C}_4)$ of the trienyl system of (Z)-1,3,5-hexatriene, in steps of 10° in the range of 180° to 0° , with energy minimization at the B3LYP/6-31+G(d) level, results in significant changes in the electronic energy (ΔE) (Figure 3A). A second minimum at $\varphi = 40^\circ$ was observed with $\Delta G = 2.37 \text{ kcal}\cdot\text{mol}^{-1}$ higher than that of the $\varphi = 180^\circ$ conformer. The significant ΔG energy difference of the two low-energy conformers with $\varphi = 40^\circ$ and $\varphi = 180.0^\circ$ shows that the $\delta_{\text{calc}}(^1\text{H})$ data (at the GIAO/B3LYP/6-311+G(2d,p) level), weighted by the respective Boltzmann factor, are nearly identical with those of the $\varphi = 180.0^\circ$ conformer. The effect of the population of the $\varphi = 40^\circ$ conformer can, thus, be neglected. The effect of variation of the torsion angle φ on ^1H NMR chemical shifts is shown in Figure 3B and Table S5. The $\delta_{\text{calc}}(^1\text{H})$ data indicate similar behavior of the “inside” H2 and H5 protons with a pronounced shielding at $100^\circ < \varphi < 180^\circ$ (Figure 3B). In the range of torsion angles $0^\circ < \varphi < 100^\circ$, the H5 proton shows a strong deshielding with a maximum value of $\delta = 7.32 \text{ ppm}$ at $\varphi = 0^\circ$. This clearly demonstrates that the strong, through-space, steric interaction with the $\text{H}_{1\text{b}}$ is the primary factor that results in δ values in the range of aromatic protons. The effect of variation of the torsion angle φ of (Z)-1,3,5-hexatriene on calculated olefinic ^1H NMR chemical shifts using the same level of theory as geometry optimization (APFD/6-311++G(d,p)) is shown in Figure S4 and Table S6. The results are very similar to those of Figure 3 and Table S5; however, the ΔE and ΔG values are slightly smaller and the deshielding effect is slightly more pronounced due to the dispersion interaction of the APFD functional.

The electronic energy ΔE (kcal/mol) and shielding changes due to the variation in the torsion angle $\varphi_1(\text{C}_2\text{C}_3\text{C}_4\text{C}_5)$ of the (E,Z,E)-2,4,6-octatriene (Figure 4, Table S7) are very similar to those due to the variation in the torsion angle φ of (Z)-1,3,5-hexatriene. Thus, the $\delta_{\text{calc}}(^1\text{H})$ data of the low-energy conformers, weighted by the respective Boltzmann factor, are identical with those of the $\varphi_1 = 180^\circ$ conformer. Again, the effect of variation of the φ_1 torsion angle on $\delta_{\text{calc}}(^1\text{H})$, using the same level of theory as geometry optimization (APFD/6-311++G(d,p)), is to decrease slightly the ΔE and ΔG values and increase the deshielding effect (Figure S5 and Table S8).

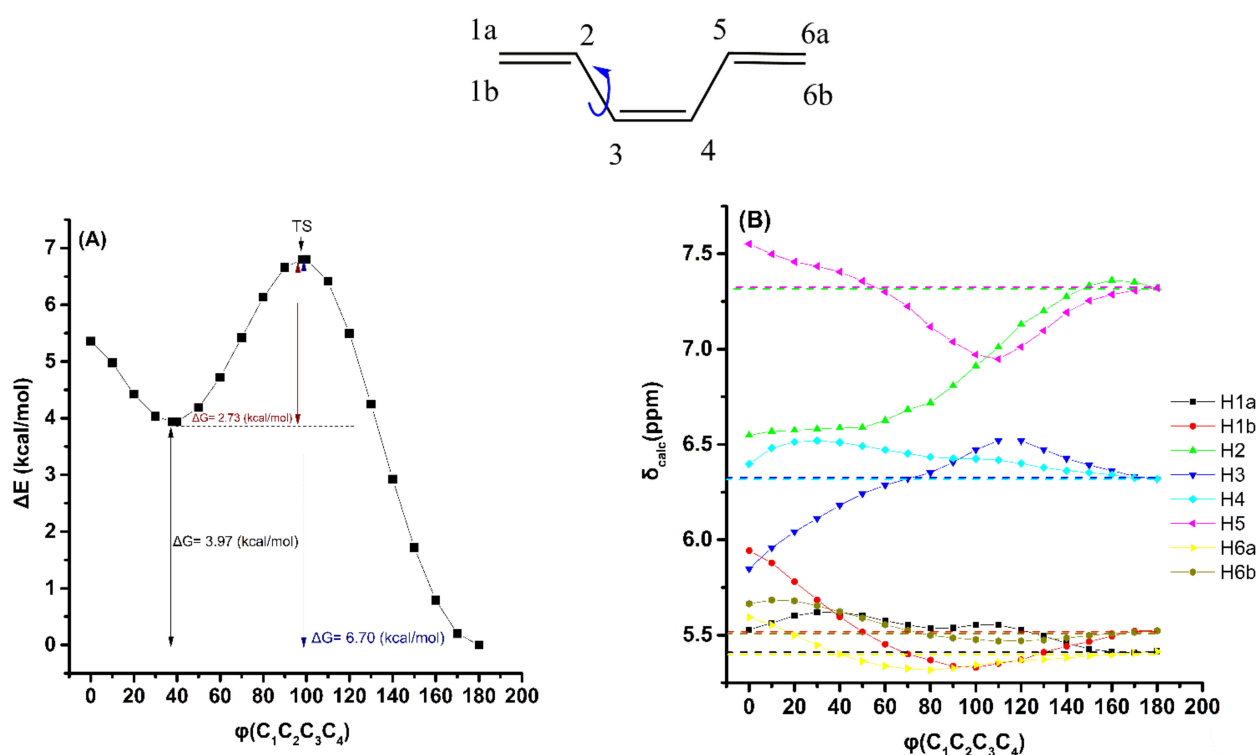


Figure 3. Effect of the variation in the torsion angle $\phi(C_1C_2C_3C_4)$ of (Z)-1,3,5-hexatriene, with energy minimization at the B3LYP/6–31+G(d) level, on the electronic energy ΔE (kcal/mol) (characteristic ΔG values are also shown) (A), and $\delta_{\text{calc}}(^1\text{H})$ data of the olefinic protons (at the GIAO/B3LYP/6–311+G(2d,p) level with CPCM in CHCl_3) (B). The experimental chemical shift values are denoted with the horizontal dotted lines.

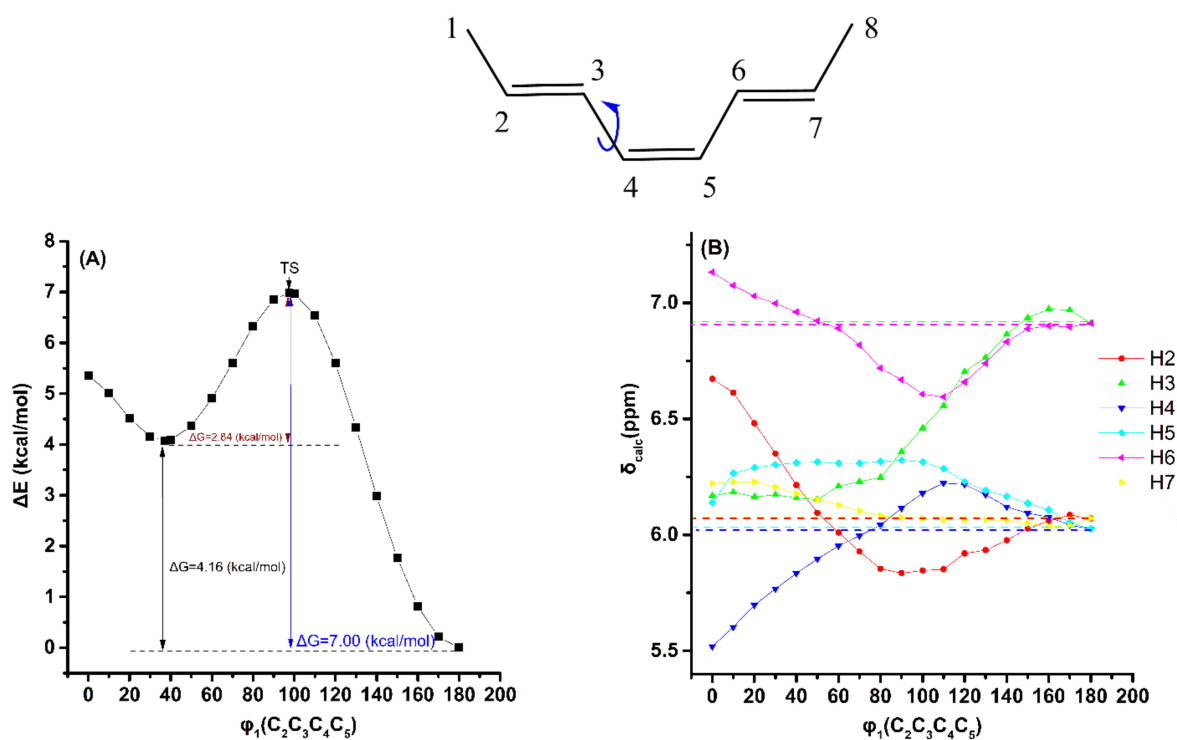


Figure 4. Effect of variation in the torsion angle $\phi_1(C_2C_3C_4C_5)$ of (E,Z,E)-2,4,6-octatriene, with energy minimization at the B3LYP/6–31+G(d) level, on the electronic energy ΔE (kcal/mol) (characteristic ΔG values are also shown) (A) and on the olefinic $\delta_{\text{calc}}(^1\text{H})$ data (at the GIAO/B3LYP/6–311+G(2d,p) level with CPCM in CHCl_3) (B). The experimental chemical shift values are denoted with the horizontal dotted lines.

The effect of the variation in the torsion angle $\varphi_2(C_1C_2C_3C_4)$ of (*E*)-1,3,5-hexatriene, with energy minimization at the B3LYP/6-31+G(d) level, on the electronic energy ΔE (kcal·mol⁻¹), and $\delta_{\text{calc}}(^1\text{H})$, at the GIAO/B3LYP/6-311+G(2d,p) level, are shown in Figure 5. A second broad minimum in the range of $\varphi_2 = 30^\circ$ to 0° was observed with $\Delta E = 3.66$ kcal·mol⁻¹ ($\Delta G = 3.28$ kcal·mol⁻¹) higher than that of the $\varphi_2 = 180.0^\circ$ conformer. The $\delta_{\text{calc}}(^1\text{H})$ values of the low-energy conformers with $\varphi_2 = 30^\circ$ to 0° and $\varphi_2 = 180.0^\circ$ (Table S9), weighted by the respective Boltzmann factors, are essentially the same as those of the $\varphi_2 = 180.0^\circ$ conformer. This is due to the negligible population of the higher minimum conformers. Of particular interest is the parallel behavior of the H₄ and H_{1b} protons as a function of the torsion angle φ_2 , with strong deshielding in the range of $0^\circ < \varphi_2 < 90^\circ$. Again, the effect of the variation in the φ_2 torsion angle on $\delta_{\text{calc}}(^1\text{H})$, using the same level of theory as geometry optimization (APFD/6-311++G(d,p)), is to decrease slightly the ΔE and ΔG values and increase the deshielding effect (Figure S6 and Table S10).

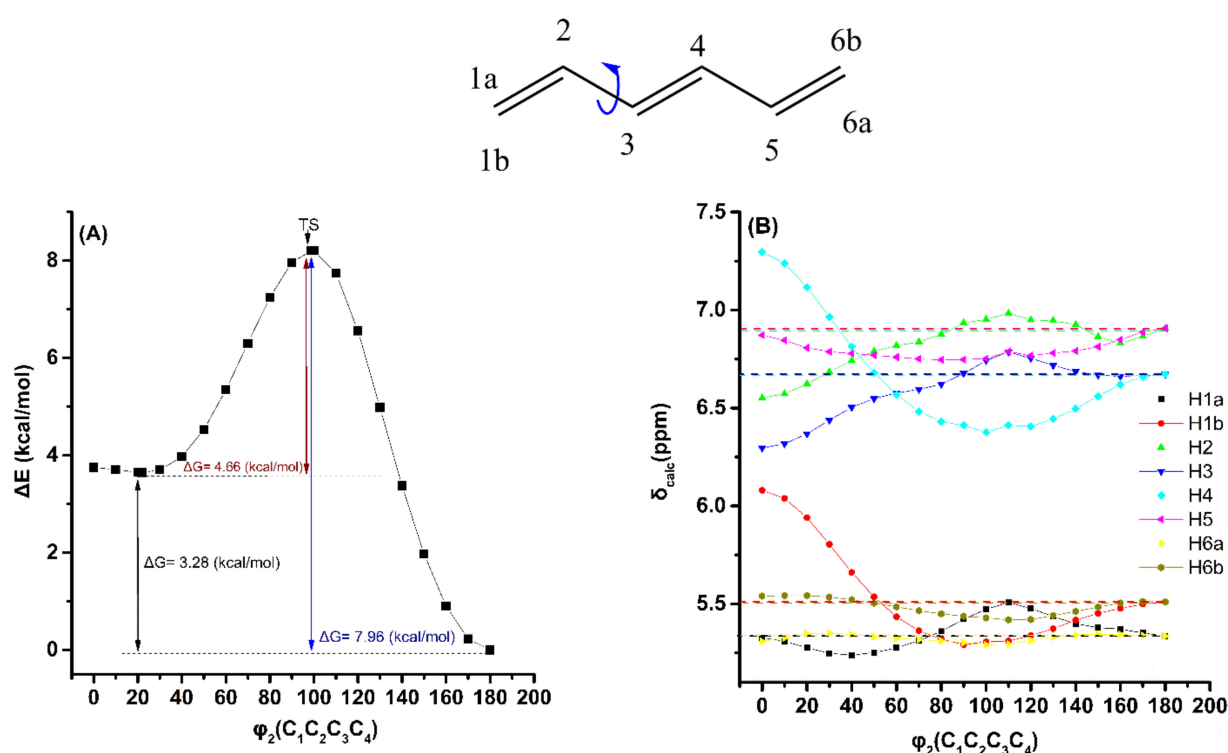


Figure 5. Effect of variation in the torsion angle $\varphi_2(C_1C_2C_3C_4)$ of (*E*)-1,3,5-hexatriene, with energy minimization at the B3LYP/6-31+G(d) level, on the electronic energy ΔE (kcal/mol) (characteristic ΔG values are also shown) (A) and on the olefinic $\delta_{\text{calc}}(^1\text{H})$ data (at the GIAO/B3LYP/6-311+G(2d,p) level with CPCM in CHCl_3) (B). The experimental chemical shift values are denoted with the horizontal dotted lines.

Figure 6 shows the effect of variation in the torsion angle $\varphi_3(C_2C_3C_4C_5)$ of the (*E,E,E*)-2,4,6-octatriene, with energy minimization at the B3LYP/6-31+G(d) level, on the electronic energy ΔE , and the computational olefinic ^1H NMR chemical shifts (at the GIAO/B3LYP/6-311+G(2d,p) level with CPCM in CHCl_3). As in the case of (*E*)-1,3,5-hexatriene, a second broad minimum in the range of $\varphi_3 = 30^\circ$ to 0° was observed with $\Delta E = 3.68$ kcal·mol⁻¹ ($\Delta G = 3.42$ kcal·mol⁻¹). The $\delta_{\text{exp}}(^1\text{H})$ data of the olefinic protons (Table S1) are in excellent agreement with the $\delta_{\text{calc}}(^1\text{H})$ values of the minimum energy conformer with $\varphi_3 = 180.0^\circ$. The $\delta_{\text{calc}}(^1\text{H})$ values of the low-energy conformers (Table S11), weighted by the respective Boltzmann factor, are essentially the same as those of the $\varphi_3 = 180.0^\circ$ conformer. This demonstrates that the weights of the higher minimum conformers are of minor importance. As in the previous cases, the effect of variation in the φ_3 torsion angle on $\delta_{\text{calc}}(^1\text{H})$ of the olefinic protons, using the same level of theory as geometry optimization (APFD/6-

311++G(d,p)), is to decrease slightly the ΔE and ΔG values and increase the deshielding effect (Figure S7 and Table S12).

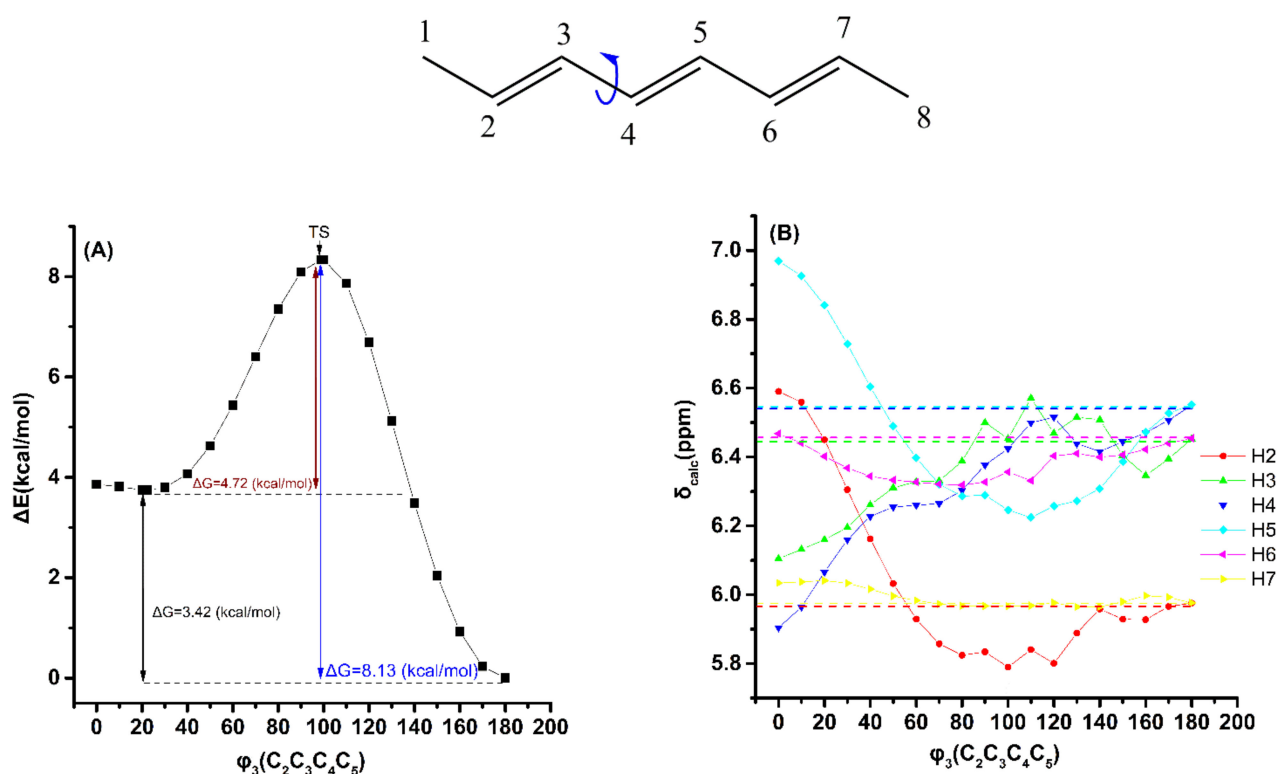


Figure 6. Effect of variation in the torsion angle φ_3 ($C_2C_3C_4C_5$) of (*E,E,E*)-2,4,6-octatriene, with energy minimization at the B3LYP/6–31+G(d) level, on the electronic energy ΔE (kcal/mol) (characteristic ΔG values are also shown) (A) and on $\delta_{\text{calc}}(^1\text{H})$ data of the olefinic protons (at the GIAO/B3LYP/6–311+G(2d,p) level of theory with CPCM in CCl_4) (B). The experimental chemical shift values are denoted with the horizontal dotted lines.

It can, therefore, be concluded that $\delta_{\text{exp}}(^1\text{H})$ are reproduced very accurately for the lowest-energy DFT-optimized single conformer. The other low-energy conformers have negligible effects on the $\delta_{\text{calc}}(^1\text{H})$ data of the conjugated olefinic protons. Furthermore, the minor functional dependence can result in the levels of accuracy that are necessary for structure elucidation in solution (see below).

Abraham et al. [50] showed that there is a deshielding effect above the $\text{C}=\text{C}$ bond at short distances, due to the van der Waals term, and a deshielding effect in the plane of the $\text{C}=\text{C}$ bond [57]. Figure S8 illustrates a plot of NBO bond order of the olefinic $\text{C}-\text{H}$ bonds vs. $\delta_{\text{calc}}(^1\text{H})$. The resulting very poor correlation ($R^2 = 0.554$) shows that the NBO bond order is not a significant factor that determines $\delta_{\text{calc}}(^1\text{H})$. Furthermore, no functional relationship was found for NBO charge densities of the olefinic $\text{C}-\text{H}$ protons vs. $\delta_{\text{calc}}(^1\text{H})$. A detailed experimental and computational (with the CHARGE 7 model) study by Abraham et al. [50,57] showed a steric deshielding effect on both alkene and aromatic ring protons, contrary to a shielding effect of $\text{H}\cdots\text{H}$ steric interactions in alkanes. All these steric interactions were described by a simple r^{-6} dependence,

$$\delta_{\text{steric}} = a_s / r^6$$

where a_s is a constant of the given hybridization of the atom. Figure S9 and Figure S10 show that, in most cases, an r^{-n} dependence is observed, which for $\text{H}\cdots\text{H}$ distances shorter than those of the van der Waals radius of the hydrogen atom ($\sim 1.2 \text{ \AA}$), becomes approximately a linear correlation. According to the semi empirical model of Cheney [51], a much better agreement with the experimental deshielding effect was obtained by correlation with

$f(r_i, \theta_i)$ than with the exponential $\exp(-ar_i)$ term, where r_i is the distance between the interacting pair of hydrogens and θ_i is the angle between H...H internuclear line and the H-C bond of interest. The above results clearly demonstrate that the deshielding effect due to non-bonded H...H repulsive interaction is a primary factor affecting $\delta(^1\text{H})$ in the trienyl systems reported therein, as in the case of simple alkenes, conjugated dienyl, and aromatic systems [47,50,51,57].

2.3. DFT-Calculated vs. Experimental ^1H NMR Chemical Shifts: Structure Elucidation in Solution of Geometric Isomers of 18:3 Conjugated Linolenic Acids and Hexadecatrienyl Pheromones

Table 2 shows conformational properties, ΔG values ($\text{kcal}\cdot\text{mol}^{-1}$) and % populations of various low-energy conformers of the 18:3 ω -5 CLA with energy minimization at the B3LYP/6-31+G(d) and APFD/6-31+G(d) levels. The structures of five low-energy conformers (A), (B), (C), (D), and (E) of β -eleostearic acid and the definition of various torsion angles are shown in Figures 7 and 8, respectively. The general tendency of the torsion angles $\varphi(\text{C}_7\text{C}_8\text{C}_9\text{C}_{10})$ and $\varphi(\text{C}_{13}\text{C}_{14}\text{C}_{15}\text{C}_{16})$, which involve the allylic C(8) and C(14) carbons, respectively, is to adopt a low-energy gauche conformation, also known as skew ($S = 120^\circ$) or skew' ($S' = -120^\circ$). On the contrary, the eclipsed syn conformation ($\varphi = 0^\circ$) results in high energy and, thus, low population (Table 2). The results are very similar for both B3LYP/6-31+G(d) and APFD/6-31+G(d) levels. An anti-zigzag conformational behavior was observed for the two polymethylene $(\text{CH}_2)_n$ groups, which are attached to the conjugated trienyl system, for all conformers of the geometric isomers of 18:3 ω -5 CLA for both B3LYP/6-31+G(d) and APFD/6-31+G(d) levels (Table 2 and Figure S11).

Table 2. Conformational properties, ΔG values ($\text{kcal}\cdot\text{mol}^{-1}$), and % populations of various low-energy conformers of the 9,11,13-conjugated fatty acid and 10,12,14-conjugated hexadecatrienyl acetate geometric isomers with geometry optimization at the B3LYP/6-31+G(d) and APFD/6-31+G(d) levels.

| Compound | Conformer | B3LYP/6-31+G(d) | | | APFD/6-31+G(d) | | |
|---|-----------|---|--|--|---|--|--|
| | | $\varphi_{\text{C}7\text{C}8\text{C}9\text{C}10}$ ($^\circ$) | $\varphi_{\text{C}13\text{C}14\text{C}15\text{C}16}$ ($^\circ$) | ΔG (kcal/mol) (% Population) | $\varphi_{\text{C}7\text{C}8\text{C}9\text{C}10}$ ($^\circ$) | $\varphi_{\text{C}13\text{C}14\text{C}15\text{C}16}$ ($^\circ$) | ΔG (kcal/mol) (% Population) |
| 9E,11E,13E Isomer (β -Eleostearic acid) | A | 120.26 (S) | 118.59 (S) | +0.36 (33.41) | 119.21 (S) | 117.99 (S) | +0.16 (38.68) |
| | B | 120.11 (S) | -119.97 (S') | 0.00 (61.35) | 118.73 (S) | -118.59 (S') | 0.00 (50.67) |
| | C | -0.78 (Syn) | -0.03 (Syn) | +3.00 (0.39) | -0.59 (Syn) | -0.11 (Syn) | +2.13 (1.39) |
| | D | -117.53 (S') | -0.83 (Syn) | +1.89 (2.53) | -116.94 (S') | -0.62 (Syn) | +1.38 (4.94) |
| | E | -0.75 (Syn) | -118.55 (S') | +1.94 (2.32) | -0.58 (Syn) | -117.27 (S') | +1.46 (4.31) |
| 9Z,11E,13E Isomer (β -Eleostearic acid) | A | 116.67 (S) | 119.18 (S) | +0.03 (25.07) | 111.25 (S) | 117.87 (S) | 0.00 (36.53) |
| | B | -118.92 (S') | -119.37 (S') | +0.15 (20.48) | -114.31 (S') | -117.53 (S') | +0.48 (16.25) |
| | C | 116.88 (S) | -119.16 (S') | +0.02 (25.50) | 112.96 (S) | -117.54 (S') | +0.18 (26.96) |
| | D | -118.88 (S') | 119.28 (S) | 0.00 (26.38) | -113.83 (S') | 118.32 (S) | +0.47 (16.52) |
| | E | -119.43 (S') | -0.76 (Syn) | +1.38 (2.57) | -113.80 (S') | -0.22 (Syn) | +1.35 (3.74) |

Table 2. Cont.

| Compound | Conformer | B3LYP/6-31+G(d) | | | APFD/6-31+G(d) | | |
|--|-----------|------------------------------|---------------------------------|--|------------------------------|---------------------------------|--|
| | | $\varphi_{c7c8c9c10}$ (°) | $\varphi_{c13c14c15c16}$ (°) | ΔG (kcal/mol) (% Population) | $\varphi_{c7c8c9c10}$ (°) | $\varphi_{c13c14c15c16}$ (°) | ΔG (kcal/mol) (% Population) |
| 9Z,11E,13Z Isomer (Punicic acid) | A | 117.46 (S) | 119.33 (S) | 0.00 (38.54) | 113.45 (S) | 114.70 (S) | 0.00 (44.84) |
| | B | 117.76 (S) | -118.63 (S') | +0.08 (33.67) | 112.18 (S) | -112.33 (S') | +0.31 (26.57) |
| | C | -119.22 (S') | 119.55 (S) | +0.27 (24.43) | -113.43 (S') | 113.54 (S) | +0.27 (28.43) |
| | D | 1.52 | -121.09 (S') | +3.83 (1.51) | 5.34 | -110.17 (S') | +3.77 (0.08) |
| | E | 117.81 (S) | 2.02 (Syn) | +3.63 (1.85) | 111.01 (S) | 4.55 (Syn) | +3.78 (0.08) |
| 10E,12E,14Z- Hexadecatrienyl acetate | A | 120.04 (S) | | +0.28 (25.59) | 118.73 (S) | | +0.08 (28.88) |
| | B | -119.39 (S') | | 0.00 (41.05) | -118.73 (S') | | +0.03 (31.42) |
| | C | 120.03 (S) | | +0.20 (29.29) | 118.73 (S) | | 0.00 (33.05) |
| | D | 1.56 (Syn) | | +1.37 (4.07) | 1.16 (Syn) | | +0.95 (6.65) |
| 10E,12Z,14Z- Hexadecatrienyl acetate | A | 119.67 (S) | | +0.44 (22.44) | 118.45 (S) | | +0.20 (26.06) |
| | B | -119.64 (S') | | 0.00 (47.15) | -118.86 (S') | | 0.00 (36.52) |
| | C | 119.56 (S) | | +0.35 (26.12) | 118.28 (S) | | +0.12 (29.82) |
| | D | 1.22 (Syn) | | +1.42 (4.29) | 0.87 (Syn) | | +0.93 (7.60) |
| 10Z,12Z,14E- Hexadecatrienyl acetate | A | 119.01 (S) | | 0.00 (30.52) | 112.30 (S) | | +0.04 (20.48) |
| | B | -119.51 (S') | | +0.51 (12.91) | -113.47 (S') | | +0.10 (18.51) |
| | C | 118.80 (S) | | 0.00 (30.52) | 112.24 (S) | | 0.00 (21.92) |
| | D | -119.50 (S') | | +0.48 (13.57) | -113.16 (S') | | +0.02 (21.19) |
| 10Z,12E,14E- Hexadecatrienyl acetate | A | 119.05 (S) | | 0.00 (31.98) | 113.03 (S) | | 0.00 (33.79) |
| | B | -121.15 (S') | | +0.54 (12.85) | -116.62 (S') | | +0.63 (11.67) |
| | C | 118.73 (S) | | +0.04 (29.89) | 113.00 (S) | | +0.04 (31.59) |
| | D | -121.06 (S') | | +0.56 (12.43) | -116.57 (S') | | +0.65 (11.28) |

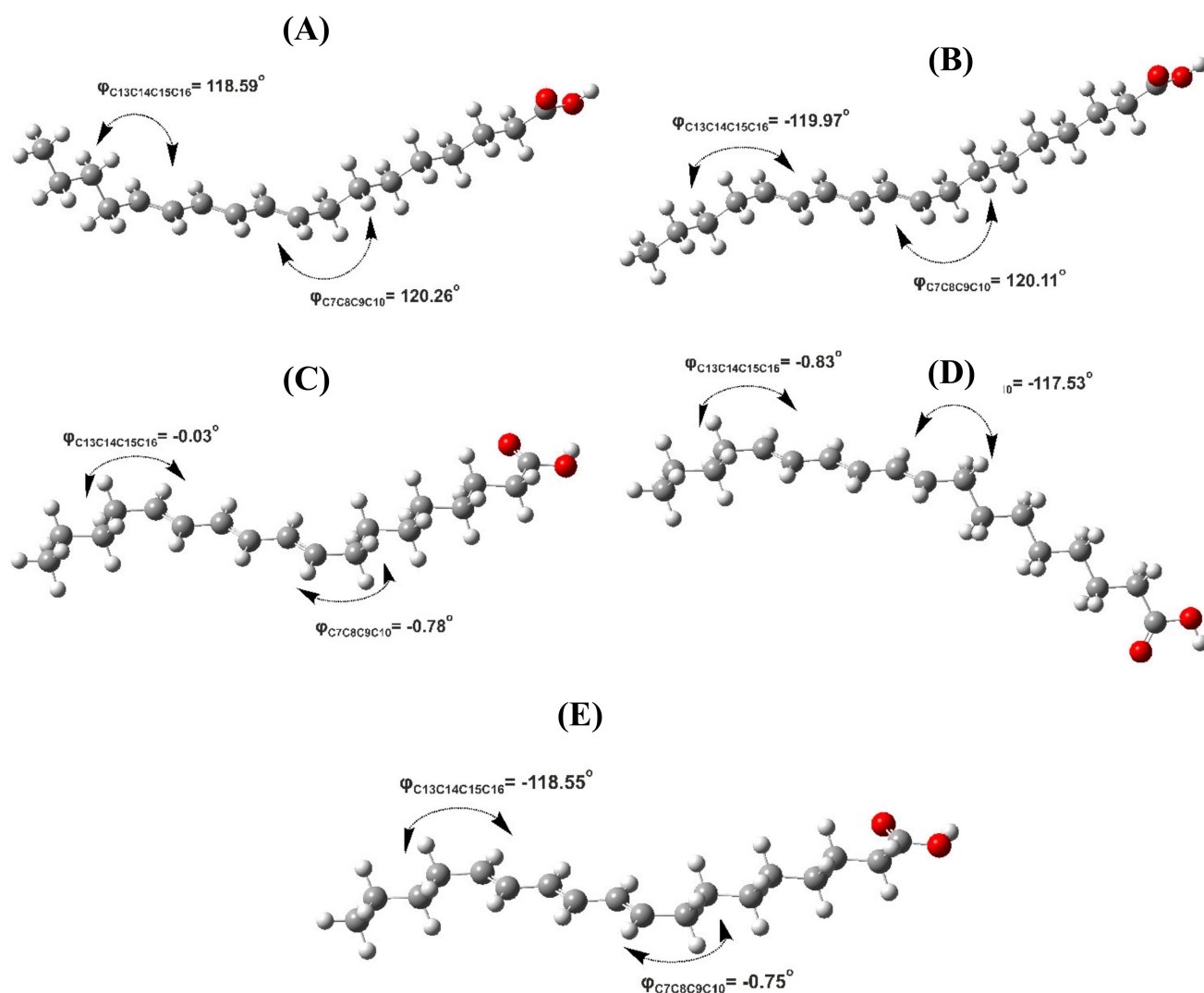
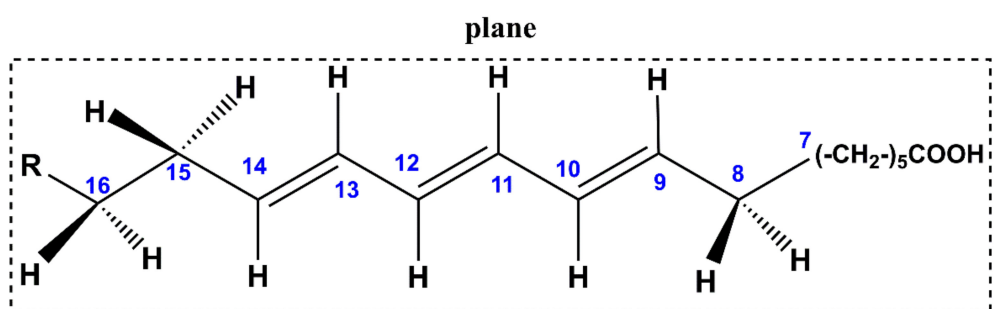
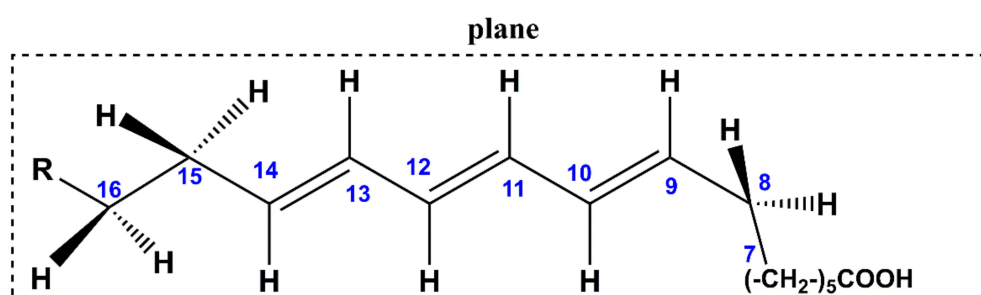


Figure 7. Structures of various conformers (A–E) of the β -eleostearic acid (9E,11E,13E-isomer) with energy minimization in the gas phase at the B3LYP/6–31+G(d) level of theory. ΔG values ($\text{kcal}\cdot\text{mol}^{-1}$) and % populations of conformers (A–E) are shown in Table 2.

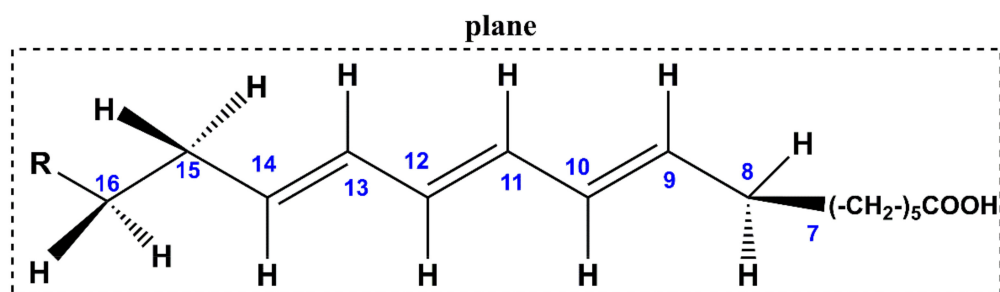
Crystallographic data for *cis*-monounsaturated fatty acids [58–60] revealed that the zigzag (anti) conformation of the polymethylene chains $(\text{CH}_2)_n$ is the most rigid and stable, whereas the gauche conformer is less stable, in agreement with our computational data. For the allylic carbons, the most stable conformations are skew (*S*) and skew' (*S'*) in the γ -crystallization form, again in agreement with our computational data of Table 2. However, the anti-*cis*-anti and skew-*cis*-anti conformations have been observed in the α - and β -crystallization forms, respectively [58]. The formation of these high-energy conformers can be attributed to specific crystal packing interactions, which are absent in solution.



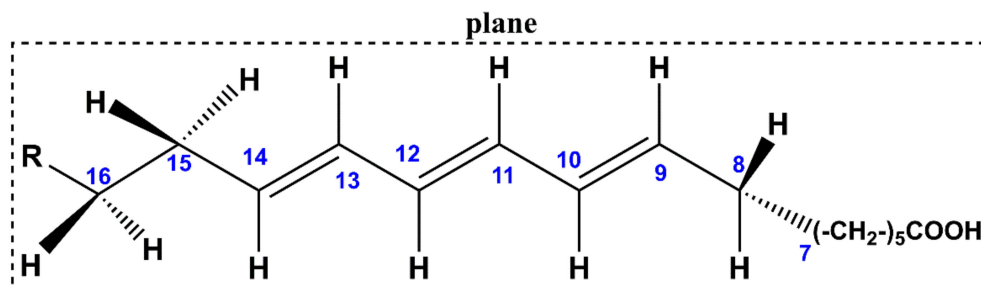
Anti: $\varphi(C_{10}C_9C_8C_7) = 180^\circ$



Syn: $\varphi(C_{10}C_9C_8C_7) = 0^\circ$



Skew: $\varphi(C_{10}C_9C_8C_7) = 120^\circ$



Skew': $\varphi(C_{10}C_9C_8C_7) = -120^\circ$

Figure 8. Definition of various conformations of the allylic carbon C8 of β -eleostearic acid (9E,11E,13E isomer).

Figure S12 shows a graphical presentation of the calculated ^1H NMR chemical shifts (at the GIAO/B3LYP/6-311+G(2d,p) (CPCM, CHCl_3) level), weighted by the respective Boltzmann factors of the various conformers of Table 2 vs. experimental chemical shifts (Table 1 and Table S13) of the three geometric isomers of the 9,11,13-CLA. The experimental chemical shifts of the H11 and H12 of β -eleostearic acid [18] deviate from linearity. Revision of the literature assignment so that H12 is deshielded to a larger degree than H11 results in very good agreement with the computational data and significant improvement of the statistical data (Table S13 and Table S14). Similar results were obtained with calculations of ^1H NMR chemical shifts using the same level of theory as geometry optimization (APFD/6-31+G(d) level) (Table S14).

Table 2 shows conformational properties, ΔG values ($\text{kcal}\cdot\text{mol}^{-1}$), and % populations of various low-energy conformers of the 10,12,14-conjugated hexadecatrienyl acetate geometric isomers with geometry optimization at the B3LYP/6-31+G(d) and APFD/6-31+G(d) levels. As in the case of CLnAs, the torsion angle $\varphi(\text{C}_7\text{C}_8\text{C}_9\text{C}_{10})$ adopts a low-energy skew (120°) or skew' (120°) conformation. On the contrary, the eclipsed syn conformation with φ angles around 0° results in high energy and, thus, low population. Figure S13 and Table S15 and Table S16 show an improvement in the correlation of δ_{calc} vs. δ_{exp} when the literature experimental chemical shifts of H13 and H15 of 9Z,11Z,13E and H13 and H14 of 9Z,11E,13E-conjugated hexadecatrienyl acetates (Table 1, [13]) have been revised (Figure S14). Similar results were obtained with the calculation of ^1H NMR chemical shifts using the same level of theory as geometry optimization (APFD/6-31+G(d) level) (Tables S15 and S16).

Figure 9 and Table 3 show that a significant improvement can be achieved in the linear regression correlation coefficient and mean square error of the correlation δ_{calc} vs. δ_{exp} of the olefinic protons of all the compounds of Figure 1 when the literature experimental chemical shifts of the compounds shown in Figure S14 have been revised. This clearly demonstrates that the accuracy of the DFT ^1H NMR shift prediction can be used to resolve ambiguities in resonance assignment.

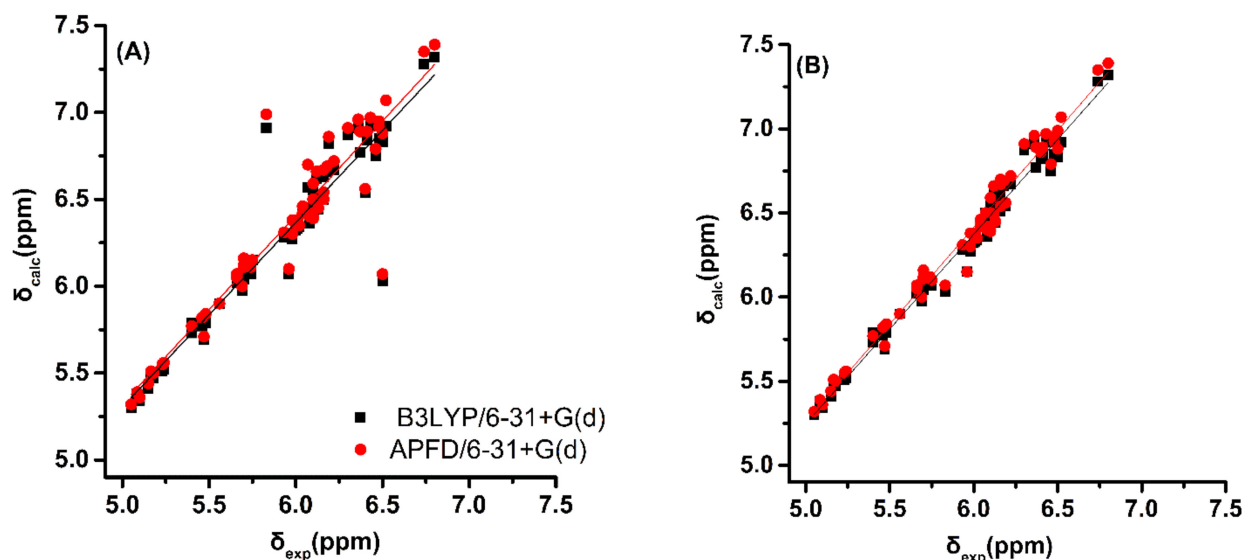


Figure 9. (A) Calculated, δ_{calc} , ^1H NMR chemical shifts of the olefinic protons, at the GIAO/B3LYP/6-311+G(2d,p) level with CPCM vs. experimental, δ_{exp} , chemical shifts with energy minimization using B3LYP/6-31+G(d) and APFD/6-31+G(d) for (*Z*)-1,3,5-hexatriene, (*E*)-1,3,5-hexatriene, (*E,Z,E*)-2,4,6-octatriene, (*E,E,E*)-2,4,6-octatriene, α -oleostearic acid (9Z, 11E, 13E), β -oleostearic acid (9E, 11E, 13E), punicic acid (9Z, 11E, 13Z), and (10E, 12E, 14Z)-, (10E,12Z,14Z)-, (10Z, 12Z, 14E)-, and (10Z, 12E, 14E)-hexatrienyl acetates. (B) The same as in (A); however, the literature experimental chemical shift data (δ_{exp}) of the compounds shown in Figure S14 have been revised.

Table 3. Linear regression correlation coefficient, mean square error, intercept, and slope of the calculated vs. experimental olefinic ^1H NMR chemical shifts of Figure 9.

| Minimization Method | Correlation Coefficient (R^2) | Mean Square Error | Intercept | Slope |
|------------------------------|-----------------------------------|-------------------|----------------|---------------|
| B3LYP/6-31+G(d) ^a | 0.873 | 0.037 | −0.002 | 1.062 |
| APFD/6-31+G(d) ^a | 0.868 (0.825) | 0.041(0.044) | −0.102 (0.518) | 1.085 (0.956) |
| B3LYP/6-31+G(d) ^b | 0.984 | 0.005 | −0.387 | 1.127 |
| APFD/6-31+G(d) ^b | 0.982 (0.942) | 0.005 (0.015) | −0.506 (0.138) | 1.153 (1.020) |

^a Data of Figure 9A; calculation of ^1H NMR chemical shifts at the GIAO/B3LYP/6-311+G(2d,p) level and ^b data of Figure 9B; calculation of ^1H NMR chemical shifts at the GIAO/B3LYP/6-311+G(2d,p) level. The data in parenthesis were obtained at the GIAO with the same level of theory as geometry optimization.

3. Computational Methods

The computational study was performed using the Gaussian 09 Rev. D.01 software [61]. The initial structures of the model triethyl compounds (*Z*)-1,3,5-hexatriene, (*E*)-1,3,5-hexatriene, (*E,Z,E*)-2,4,6-octatriene, and (*E,E,E*)-2,4,6-octatriene were drawn using the GaussView program and were energy minimized at the B3LYP/6-31+G(d), B3LYP/6-311++G(d,p), B3LYP-D3/6-31+G(d), B3LYP-D3/6-311++G(d,p) (the D3 version of Grimme dispersion with Becke–Johnson damping), APFD/6-31+G(d), APFD/6-311++G(d,p), PBE0/6-31+G(d), PBE0/6-311++G(d,p), M06-2X/6-31+G(d), M06-2X/6-311++G(d,p), ω B97XD/6-31+G(d), and ω B97XD/6-311++G(d,p) levels (gas phase). In the case of α -oleostearic acid (9*Z*, 11*E*, 13*E*), β -oleostearic acid (9*E*, 11*E*, 13*E*), punicic acid (9*Z*, 11*E*, 13*Z*), (10*E*, 12*E*, 14*Z*)-, (10*E*,12*Z*,14*Z*)-, (10*Z*, 12*Z*, 14*E*)-, and (10*Z*, 12*E*, 14*E*)-hexatrienyl acetates, a conformational analysis was, firstly, performed by rotation of the aliphatic carbons of the $(\text{CH}_2)_n$ chains, which constitute with the rigid conjugated double bonds a flat system. The resulting conformers were energy minimized with DFT at the B3LYP/6-31+G(d) and APFD/6-31+G(d) levels, while the subsequent energy minimization of the selected stable structures was carried out at the same level of calculation. The optimized geometries were verified by performing frequency calculation at the same level (zero imaginary frequencies). The scanning of torsional angles was performed using the redundant coordinates in Gaussian 09 [47]. ΔG values were calculated from the thermochemistry results, either between the stable conformers or between the stable conformers and the corresponding transition states. The computed proton chemical shifts were performed using (i) a single methodology at the GIAO/B3LYP/6-311+G(2d,p) level and (ii) GIAO at the same level of theory as geometry optimization. In both cases, the conductor-like polarizable continuum model (CPCM) was used in CHCl_3 or CCl_4 , for experimental values obtained in CDCl_3 and CCl_4 , respectively (Table S1 and Table S2). $\delta_{\text{calc}}(^1\text{H})$ were referenced with respect to the standard TMS, which was optimized at the same level (Table S17).

4. Conclusions

From the DFT data of the trienyl conjugated compounds of Figure 1 reported therein, it can be concluded that:

- Very good linear correlations can be obtained between DFT-calculated and experimental ^1H NMR chemical shifts of the olefinic protons of the lowest-energy DFT-optimized single conformer using standard functionals (B3LYP and PBE0) as well as corrections for dispersion interactions (B3LYP-D3, APFD, M06-2X and ω B97XD). The ω B97XD performs slightly better, but again the accuracy of the functionals used was rather similar.
- Through-space $\text{H} \cdots \text{H}$ steric interaction is the primary factor that results in strong deshielding of closely spaced trienyl olefinic protons, in excellent agreement with literature data on alkenes and aromatic systems [50,51,57].

- (c) The accuracy of computational ^1H NMR chemical shifts can facilitate (i) the unequivocal assignment of the geometric isomerism in conjugated trienyl systems of biological systems, such as CLnAs and hexadecatrienyl pheromones, and especially in the case of problematic resonance assignment due to extensive signal overlap, and (ii) structure elucidation in solution [28,36].

Supplementary Materials: Figure S1: Calculated ^1H NMR chemical shifts vs. experimental chemical shifts, Figure S2: Calculated ^1H NMR chemical shifts vs. experimental chemical shifts, Figure S3: Calculated ^1H NMR chemical shifts vs. experimental chemical shifts, Figure S4: Effect of variation of the torsion angle φ ($\text{C}_1\text{C}_2\text{C}_3\text{C}_4$), Figure S5: Effect of variation of the torsion angle φ_1 ($\text{C}_2\text{C}_3\text{C}_4\text{C}_5$), Figure S6: Effect of variation of the torsion angle φ_2 ($\text{C}_1\text{C}_2\text{C}_3\text{C}_4$), Figure S7: Effect of variation of the torsion angle φ_3 ($\text{C}_2\text{C}_3\text{C}_4\text{C}_5$), Figure S8: NBO bond order of the olefinic C-H bonds vs. calculated ^1H NMR chemical shifts, Figure S9: The dependence of $\delta(^1\text{H})$ vs. distance, Figure S10: The dependence of $\delta(^1\text{H})$ vs. distance, Figure S11: Structures of various conformers of the punicic acid, Figure S12: Graphical presentation of calculated ^1H NMR chemical shifts vs. experimental values, Figure S13: Graphical presentation of calculated ^1H NMR chemical shifts vs. experimental values, Figure S14: Experimental ^1H NMR and calculated chemical shifts, Table S1: Experimental and computational ^1H NMR chemical shifts, Table S2: Experimental and computational ^1H NMR chemical shifts, Table S3: Statistical data of calculated vs. experimental ^1H chemical shifts, Table S4: Statistical data of calculated vs. experimental ^1H chemical shifts, Table S5: Effect of variation of the torsion angle φ_1 ($\text{C}_2\text{C}_3\text{C}_4$) on calculated ^1H NMR chemical shifts, Table S6: Effect of variation of the torsion angle φ ($\text{C}_1\text{C}_2\text{C}_3\text{C}_4$) on calculated ^1H NMR chemical shifts, Table S7: Effect of variation of the $\text{C}_2\text{C}_3\text{C}_4\text{C}_5$ torsion angle on calculated ^1H NMR chemical shifts, Table S8: Effect of variation of the $\text{C}_2\text{C}_3\text{C}_4\text{C}_5$ torsion angle on calculated ^1H NMR chemical shifts, Table S9: Effect of variation of the $\text{C}_1\text{C}_2\text{C}_3\text{C}_4$ torsion angle on calculated ^1H NMR chemical shifts, Table S10: Effect of variation of the $\text{C}_1\text{C}_2\text{C}_3\text{C}_4$ torsion angle on calculated ^1H NMR chemical shifts, Table S11: Effect of variation of the $\text{C}_2\text{C}_3\text{C}_4\text{C}_5$ torsion angle on calculated ^1H NMR chemical shifts, Table S12: Effect of variation of the $\text{C}_2\text{C}_3\text{C}_4\text{C}_5$ torsion angle on calculated ^1H NMR chemical shifts, Table S13: Calculated and experimental ^1H NMR chemical shifts, Table S14: Statistical analysis of the chemical shift data, Table S15: Calculated and experimental ^1H NMR chemical shifts, Table S16: Statistical analysis of the chemical shift data, Table S17: Calculated shielding values of the reference TMS molecule.

Author Contributions: T.V., C.O., and M.G.S. performed DFT calculations; A.P. performed literature search; M.G.S. and I.P.G. conceived and designed the study and contributed to the writing of the manuscript. All authors have read and approved the final manuscript.

Funding: I.P.G. received funding from the Hellenic Foundation for Research and Innovation (H.F.R.I.) under the “First Call for H.F.R.I. Research Projects to support Faculty members and Researchers and the procurement of high-cost research equipment grant” (Project Number: 2050).

Conflicts of Interest: The authors declare that they have no conflict of interest.

Sample Availability: Samples of the compounds are not available from the authors.

References

1. Yuan, G.F.; Chena, X.E.; Li, D. Conjugated linolenic acids and their bioactivities: A review. *Food Funct.* **2014**, *5*, 1360–1368. [[CrossRef](#)]
2. Dubey, K.K.D.; Sharma, G.; Kumar, A. Conjugated linolenic acids: Implication in cancer. *J. Agric. Food Chem.* **2019**, *67*, 6091–6101. [[CrossRef](#)] [[PubMed](#)]
3. Igarashi, M.; Miyazawa, T. Newly recognized cytotoxic effect of conjugated trienoic fatty acids on cultured human tumor cells. *Cancer Lett.* **2000**, *148*, 173–179. [[CrossRef](#)]
4. Özgül-Yücel, S. Determination of conjugated linolenic acid content of selected oil seeds grown in Turkey. *J. Am. Oil Chem. Soc.* **2005**, *82*, 893–897. [[CrossRef](#)]
5. Yasui, Y.; Hosokawa, M.; Kohno, H. Growth inhibition and apoptosis induction by all-*trans*-conjugated linolenic acids on human colon cancer cells. *Anticancer Res.* **2006**, 1855–1860.
6. Grossmann, M.E.; Mizuno, N.K.; Schuster, T.; Cleary, M.P. Punicic acid is an ω -5 fatty acid capable of inhibiting breast cancer proliferation. *Int. J. Oncol.* **2009**, *36*, 421–426.
7. Lansky, E.P.; Newman, R.A. *Punica granatum* (Pomegranate) and its potential for prevention and treatment of inflammation and cancer. *J. Ethnopharmacol.* **2007**, *109*, 177–206. [[CrossRef](#)]

8. Aruna, P.; Venkataramanamma, D.; Singh, A.K.; Singh, R.P. Health benefits of puniceic acid: A review. *Compr. Rev. Food Sci. Food Saf.* **2016**, *15*, 16–27. [[CrossRef](#)]
9. Suzuki, R.; Noguchi, R.; Ota, T.; Abe, M.; Miyashita, K.; Kawada, T. Cytotoxic effect of conjugated trienoic fatty acids on mouse tumor and human monocytic leukemia cells. *Lipids* **2001**, *36*, 477–482. [[CrossRef](#)]
10. Seol, K.Y.; Honda, H.; Usui, K.; Ando, T.; Matsumoto, Y. 10,12,14-Hexadecatrienyl acetate: Sex pheromone of the mulberry pyralid, *Glyphodes pyloalis* walker (Lepidoptera: Pyralidae). *Agric. Biol. Chem.* **1987**, *51*, 2285–2287. [[CrossRef](#)]
11. Gries, R.; Reckziegel, A.; Bogenschütz, H.; Kontzog, H.-G.; Schlegel, C.; Francke, W.; Millar, J.G.; Gries, G. (Z,Z)-11,13-Hexadecadienyl acetate and (Z,E)-11,13,15-hexadecatrienyl acetate: Synergistic sex pheromone components of oak processionary moth, *Thaumetopoea processionea* (Lepidoptera: Thaumetopoeidae). *Chemoecology* **2004**, *14*, 95–100. [[CrossRef](#)]
12. Millar, J.G.; McElfresh, J.S.; Romero, C.; Vila, M.; Mari-Mena, N.; Lopez-Vaamonde, C. Identification of the sex pheromone of a protected species, the Spanish moon moth *Graellsia isabellae*. *J. Chem. Ecol.* **2010**, *36*, 923–932. [[CrossRef](#)] [[PubMed](#)]
13. Ando, T.; Ogura, Y.; Koyama, M.; Kurane, M.; Uchiyama, M.; Yaul Seol, K.Y. Syntheses and NMR analyses of eight geometrical isomers of 10,12,14-hexadecatrienyl acetate, sex pheromone candidates of the mulberry pyralid. *Agric. Biol. Chem.* **1988**, *52*, 2459–2468.
14. Doolittle, R.E.; Brabham, A.; Tumlinson, J.H. Sex pheromone of *Manduca sexta* (L) stereoselective synthesis of (10E, 12E, 14Z)-10,12,14-hexadecatrienyl and isomers. *J. Chem. Ecol.* **1990**, *16*, 1131–1153. [[CrossRef](#)] [[PubMed](#)]
15. Ando, T.; Ohsawa, H. Sex pheromone candidates with a conjugated triene system: Synthesis and chemical characterization. *J. Chem. Ecol.* **1993**, *19*, 119–132. [[CrossRef](#)]
16. Tulloch, A.P.; Bergter, L. Analysis of the conjugated trienoic acid containing oil from *fevillea trilobata* by ¹³C nuclear magnetic resonance spectroscopy. *Lipids* **1979**, *14*, 996–1002. [[CrossRef](#)]
17. Cao, Y.; Gao, H.-L.; Chen, J.-N.; Chen, Z.-Y.; Yang, L. Identification and characterization of conjugated linolenic acid isomers by Ag+HPLC and NMR. *J. Agric. Food. Chem.* **2006**, *54*, 9004–9009. [[CrossRef](#)]
18. Cao, Y.; Yang, L.; Gao, H.-L.; Chen, J.-N.; Chen, Z.-Y.; Ren, Q.-S. Re-characterization of three conjugated linolenic acid isomers by GC-MS and NMR. *Chem. Phys. Lipids* **2007**, *145*, 128–133. [[CrossRef](#)]
19. Sassano, G.; Sanderson, P.; Franx, J.; Groot, P. van Straalen, J.; Bassaganya-Riera, J. Analysis of pomegranate seed oil for the presence of jacaric acid. *J. Sci. Food Agric.* **2009**, *89*, 1046–1052. [[CrossRef](#)]
20. Alexandri, E.; Ahmed, R.; Siddiqui, H.; Choudhary, M.; Tsiafoulis, C.; Gerothanassis, I.P. High resolution NMR spectroscopy as a structural and analytical tool for unsaturated lipids in solution. *Molecules* **2017**, *22*, 1663. [[CrossRef](#)]
21. Albriktsen, P.; Harris, R.K. NMR Studies of conjugated linear trienes. *Acta Chem. Scand.* **1973**, *27*, 1875–1882. [[CrossRef](#)]
22. Brouwer, A.M.; Bezemer, L.; Jacobs, H.J.C. Steric perturbation of the conjugated triene chromophore. Conformational analysis of (E)- and (2)-3-methyl-1,3,5-hexatriene and (2)-3-tert-butyl-1,3,5-hexatriene. *Red. Trav. Chim. Pays-Bas* **1992**, *111*, 138–143. [[CrossRef](#)]
23. Brouwer, A.M.; Bezemer, L.; Jacobs, H.J.C. Kinetics of thermal interconversion between cis, cis-1,3,5-octatriene, cis, cis, cis-2,4,6-octatriene, and cis, cis, trans-2,4,6-octatriene. *Red. Trav. Chim. Pays-Bas* **1998**, *53*, 1132–1137.
24. Townsend, E.M.; Schrock, R.R.; Hoveyda, A.H. Z-Selective metathesis homocoupling of 1,3-dienes by molybdenum and tungsten monoaryloxide pyrrolide (MAP) complexes. *J. Am. Chem. Soc.* **2012**, *134*, 11334–11337. [[CrossRef](#)] [[PubMed](#)]
25. Bifulco, G.; Dambruoso, P.; Gomez-Paloma, L.; Riccio, R. Determination of relative configuration in organic compounds by NMR spectroscopy and computational methods. *Chem. Rev.* **2007**, *107*, 3744–3779. [[CrossRef](#)] [[PubMed](#)]
26. Smith, S.G.; Goodman, J.M. Assigning the stereochemistry of pairs of diastereoisomers using GIAO NMR shift calculations. *J. Org. Chem.* **2009**, *74*, 4597–4607. [[CrossRef](#)] [[PubMed](#)]
27. Saielli, G.; Nicolaou, K.C.; Ortiz, A.; Zhang, H.; Bagno, A. Addressing the stereochemistry of complex organic molecules by density functional theory-NMR: Vannusal B. in retrospective. *J. Am. Chem. Soc.* **2011**, *133*, 6072–6077. [[CrossRef](#)] [[PubMed](#)]
28. Lodewyk, M.W.; Siebert, M.R.; Tantillo, D.J. Computational prediction of ¹H and ¹³C chemical shifts: A useful tool for natural product, mechanistic, and synthetic organic chemistry. *Chem. Rev.* **2012**, *112*, 1839–1862. [[CrossRef](#)]
29. Tantillo, D.J. Walking in the woods with quantum chemistry –applications of quantum chemical calculations in natural products research. *Nat. Prod. Rep.* **2013**, *30*, 1079–1086. [[CrossRef](#)] [[PubMed](#)]
30. Siskos, M.G.; Kontogianni, V.G.; Tsiafoulis, C.G.; Tzakos, A.G.; Gerothanassis, I.P. Investigation of solute–solvent interactions in phenol compounds: Accurate ab initio calculations of solvent effects on ¹H NMR chemical shifts. *Org. Biomol. Chem.* **2013**, *11*, 7400–7411. [[CrossRef](#)]
31. Willoughby, P.H.; Jansma, M.J.; Hoye, T.R. A guide to small-molecule structure assignment through computation of (¹H and ¹³C) NMR chemical shifts. *Nat. Protoc.* **2014**, *9*, 643–660. [[CrossRef](#)]
32. Jaremko, L.; Jaremko, M.; Buczek, A.; Broda, A.M.; Kupka, T.; Jackowski, K. ¹H and ¹³C shielding measurements in comparison with DFT calculations performed for 2-(acetylamino)-N,N-dimethyl-3-phenylacrylamide isomers. *Chem. Phys. Lett.* **2015**, *627*, 1–6. [[CrossRef](#)]
33. Navarro-Vázquez, A. State of the art and perspectives in the application of quantum chemical prediction of ¹H and ¹³C chemical shifts and scalar couplings for structural elucidation of organic compounds. *Magn. Reson. Chem.* **2017**, *55*, 2–32. [[CrossRef](#)] [[PubMed](#)]

34. Tarazona, G.; Bénédict, G.; Fernández, R.; Pérez, M.; Rodríguez, J.; Jiménez, C.; Cuevas, C. Can stereoclusters separated by two methylene groups be related by DFT studies? The case of the cytotoxic meroditerpeneshalioxepines. *J. Nat. Prod.* **2018**, *81*, 343–348. [[CrossRef](#)]
35. Krivdin, L.B. Computational protocols for calculating ^{13}C NMR chemical shifts. *Progr. NMR Spectrosc.* **2019**, *112–113*, 103–156. [[CrossRef](#)] [[PubMed](#)]
36. Krivdin, L.B. Computational ^1H NMR: Part 1. Theoretical background. *Magn. Reson. Chem.* **2019**, *57*, 897–914. [[CrossRef](#)]
37. Semenov, V.A.; Krivdin, L.B. Computational ^1H and ^{13}C NMR of strychnobailonine: On the way to larger molecules calculated at lower computational costs. *Magn. Reson. Chem.* **2021**, *59*, 108–116. [[CrossRef](#)] [[PubMed](#)]
38. Siskos, M.G.; Tzakos, A.G.; Gerothanassis, I.P. Accurate ab initio calculations of $\text{O-H}\cdots\text{O}$ and $\text{O-H}\cdots\text{O}$ proton chemical shifts: Towards elucidation of the nature of the hydrogen bond and prediction of hydrogen bond distances. *Org. Biomol. Chem.* **2015**, *13*, 8852–8868. [[CrossRef](#)]
39. Siskos, M.G.; Choudhary, M.I.; Tzakos, A.G.; Gerothanassis, I.P. ^1H NMR chemical shift assignment, structure and conformational elucidation of hypericin with the use of DFT calculations—The challenge of accurate positions of labile hydrogens. *Tetrahedron* **2016**, *72*, 8287–8293. [[CrossRef](#)]
40. Siskos, M.G.; Choudhary, M.I.; Gerothanassis, I.P. Hydrogen atomic positions of $\text{O-H}\cdots\text{O}$ hydrogen bonds in solution and in the solid state: The synergy of quantum chemical calculations with ^1H -NMR chemical shifts and X-ray diffraction methods. *Molecules* **2017**, *22*, 415. [[CrossRef](#)]
41. Siskos, M.G.; Choudhary, M.I.; Gerothanassis, I.P. Refinement of labile hydrogen positions based on DFT calculations of ^1H NMR chemical shifts: Comparison with X-ray and neutron diffraction methods. *Org. Biomol. Chem.* **2017**, *15*, 4655–4666. [[CrossRef](#)]
42. Siskos, M.G.; Choudhary, M.I.; Gerothanassis, I.P. DFT-calculated structures based on ^1H NMR chemical shifts in solution vs. structures solved by single-crystal X-ray and crystalline-sponge methods: Assessing specific sources of discrepancies. *Tetrahedron* **2018**, *74*, 4728–4737. [[CrossRef](#)]
43. Torralba, M.P.; Sanz, D.; Claramunt, R.M.; Alkorta, I.; Dardonville, C.; Elguero, J. The structure of fosfomicin salts in solution and in the solid state by nuclear magnetic resonance spectroscopy and DFT calculations. *Tetrahedron* **2018**, *74*, 3937–3942. [[CrossRef](#)]
44. Mari, S.H.; Varras, P.C.; Wahab, A.-t.; Choudhary, I.M.; Siskos, M.G.; Gerothanassis, I.P. Solvent-dependent structures of natural products based on the combined use of DFT calculations and ^1H -NMR chemical shifts. *Molecules* **2019**, *24*, 2290. [[CrossRef](#)]
45. Siskos, M.G.; Varras, P.C.; Gerothanassis, I.P. DFT calculations of $\text{O-H}\cdots\text{O}$ ^1H NMR chemical shifts in investigating enol–enol tautomeric equilibria: Probing the impacts of intramolecular hydrogen bonding vs. stereoelectronic interactions. *Tetrahedron* **2020**, *76*, 130979. [[CrossRef](#)]
46. Ahmed, R.; Varras, P.C.; Siskos, M.G.; Siddiqui, H.; Choudhary, M.I.; Gerothanassis, I.P. NMR and computational studies as analytical and high-resolution structural tool for complex hydroperoxides and endo-hydroperoxides of fatty acids in solution. *Molecules* **2020**, *25*, 4902. [[CrossRef](#)] [[PubMed](#)]
47. Venianakis, T.; Oikonomaki, C.; Siskos, M.G.; Varras, P.C.; Primikyri, A.; Alexandri, E.; Gerothanassis, I.P. DFT Calculations of ^1H - and ^{13}C -NMR chemical shifts of geometric isomers of conjugated linoleic acid (18:2 ω -7) and model compounds in solution. *Molecules* **2020**, *25*, 3660. [[CrossRef](#)] [[PubMed](#)]
48. Touw, S.I.E.; de Groot, H.J.M.; Buda, F. DFT calculations of the ^1H NMR chemical shifts and ^{13}C chemical shifts tensors of retinal isomers. *J. Mol. Struct. (Theochem)* **2004**, *711*, 141–147. [[CrossRef](#)]
49. Ditchfield, R. Self-consistent perturbation theory of diamagnetism I. A gauge-invariant LCAO method for N.M.R. chemical shifts. *Mol. Phys.* **1974**, *27*, 789–807. [[CrossRef](#)]
50. Abraham, R.J.; Canton, M.; Griffiths, L. Proton chemical shifts in alkenes and anisotropic and steric effects in double bond. *Magn. Reson. Chem.* **2001**, *39*, 421–431. [[CrossRef](#)]
51. Cheney, B.V. Magnetic deshielding of protons due to intramolecular steric interactions with proximate hydrogens. *J. Am. Chem. Soc.* **1968**, *90*, 5386–5390. [[CrossRef](#)]
52. Marshall, T.W.; Pople, J.A. Nuclear magnetic shielding of a hydrogen atom in an electric field. *Mol. Phys.* **1958**, *1*, 199–202. [[CrossRef](#)]
53. Cobb, T.B.; Memory, J.B. High-resolution NMR spectra of polycyclic hydrocarbons. II. Pentacyclic compounds. *J. Phys. Chem.* **1967**, *47*, 2020–2025. [[CrossRef](#)]
54. Grimme, S.; Diedrich, C.; Korth, M. The importance of inter- and intramolecular van der Waals interactions in organic reactions: The dimerization of anthracene revisited. *Angew. Chem. Int. Ed.* **2006**, *118*, 641–645. [[CrossRef](#)]
55. Hujo, W.; Grimme, S. Performance of the van der Waals density functional VV10 and (hybrid) GGA variants for thermochemistry and noncovalent interactions. *J. Chem. Theory Comput.* **2011**, *7*, 3866–3871. [[CrossRef](#)] [[PubMed](#)]
56. Kupka, T.; Stachow, M.; Nieradka, M.; Kaminsky, J.; Pluta, T. Convergence of nuclear magnetic shieldings in the Kohn-Sham limit of several small molecules. *J. Chem. Theory Comput.* **2010**, *6*, 1580–1589. [[CrossRef](#)]
57. Abraham, R.J.; Mobli, M. *Modelling ^1H NMR Spectra of Organic Compounds Theory, Applications and NMR Prediction Software*; John Wiley & Sons Ltd.: Chichester, UK, 2008.
58. Kaneko, F.; Yano, J.; Sato, K. Diversity in the fatty-acid conformation and chain packing of cis-unsaturated lipids. *Curr. Opin. Struct. Biol.* **1998**, *8*, 417–425. [[CrossRef](#)]
59. Suzuki, M.; Ogaki, T.; Sato, K. Crystallization and transformation mechanisms of α , β and γ polymorphs of ultra-pure oleic acid. *J. Am. Oil. Chem. Soc.* **1985**, *62*, 1600–1604. [[CrossRef](#)]

-
60. Kaneko, F.; Yamazaki, K.; Kitagawa, K.; Kikyo, T.; Kobayashi, M.; Sato, K.; Suzuki, M. Structure and crystallization behavior of the β phase of oleic acid. *J. Phys. Chem. B* **1997**, *101*, 1803–1809. [[CrossRef](#)]
 61. Frisch, M.J.; Trucks, G.W.; Schlegel, H.B.; Scuseria, G.E.; Robb, M.A.; Cheeseman, J.R.; Scalmani, G.; Barone, V.; Mennucci, B.; Petersson, G.A.; et al. *Gaussian 0.9, Revision. D.01*; Gaussian, Inc.: Wallingford, CT, USA, 2009.